Experimental Mechanics (2013) 53:1033–1038
DOI 10.1007/s11340-012-9709-y

Residual Stress-Related Common Intersection Points in the Mechanical Behavior of Ceramic Matrix Composites Undergoing Cyclic Loading

K.G. Dassios · T.E. Matikas

Received: 31 August 2012 / Accepted: 18 December 2012 / Published online: 19 January 2013

Abstract The mechanical response of SiC-fiber reinforced barium osumilite ceramic matrix composites tested in tension with unloading/reloading cycles was very recently reported to exhibit self-assembling common intersection points (CIP) of unloading/reloading loops in the tensile domain which relate exactly to the thermal residual stress state of reinforcing fibers in a matrix of a lower coefficient of thermal expansion (Dassios et al. Compos A: Appl Sci Manuf 44:105–113, 2013). Knowledge of the experimentally-exact residual stress state enables, herein, examination of the validity of the conventional compliance-based methodology for indirectly calculating residual stresses from projected/extrapolated CIPs. The efficiency of two prominent residual stress prediction models is also tested across the experimentally-established value of thermal residual stress (TRS). The significance of the CIP as the TRS-free origin of the stress-strain curve is discussed in view of the importance in calculating accurate material property values from mechanical testing data of materials under residual stress.

Keywords Ceramic matrix composites · Residual stresses · Cyclic load · Common intersection point

Introduction

The mechanical and thermal performance of ceramic matrix composites (CMCs) depends strongly on the sign and magnitude of internal thermal residual stresses (TRS) that develop upon cooling of the material from the crystallization temperature due to the mismatch of elastic constants and coefficients of thermal expansion (CTEs) between the composite constituents [2]. TRS directly affect interfacial conditions [3, 4] and the stress state of the matrix and reinforcing fibers [5, 6], as they also determine the type of micro-cracking [7].

To date, there are four main experimental methods for indirectly evaluating residual stresses in glass-ceramics: X-ray diffraction (XRD) [8], Raman [9, 10] and fluorescence [3, 11, 12] spectroscopy and indentation [13]. Evaluation of residual stresses in ceramic matrix composites has widely followed a separate, very popular method that relies exclusively on mechanical testing data: In the Common Intersection Point (CIP) method proposed by Camus [14] and further improved by Steen [15], the compliance slopes of unloading-reloading loops in the stress–strain curves of thus tested CMCs, meet at a single point whose coordinates directly relate to the axial TRS state of the reinforcing fibers. This CIP is the fictitious TRS-free origin of the stress/strain curve of the material. As, most often, the CIP is not visible in the tensile domain of the curves [14–17], the points have been conventionally established by extrapolation of the compliance slopes of reloading-unloading loops. Morscher et al. successfully calculated a tensile TRS state of SiC fibres in a SiC matrix, however only by application of the same compliance extrapolation method[18]. While residual stress values calculated from projected CIPs have generally compared well with theoretical predictions, it is only very recently that the mere existence of a common intersection point in cyclically-loaded CMCs with internal residual stresses was proven experimentally for the first time [1]. Knowledge of experimentally-exact TRS states introduces new challenges, such as to validate the conventional CIP-by-compliance theory and other TRS prediction models.

In the present article, the coordinates of experimental CIPs, self-assembled in the tensile domains of cyclically-loaded SiC-fibre reinforced barium osumilite ceramic matrix

K.G. Dassios (✉) · T.E. Matikas
Department of Materials Science and Engineering,
University of Ioannina, Ioannina 451 10, Greece
e-mail: kdassios@cc.uoi.gr

composites, are used to examine the efficiency of two popular TRS-prediction equations as well as to validate the leading CIP-by-compliance methodology for evaluation of residual stresses.

Experimental

Cross-ply composite laminates, 3 mm thick, were externally processed by hot-pressing prepreg sheets of SiC-Tyranno fibers (UBE Industries Ltd., Japan; quoted elastic modulus E_f=190 GPa, quoted strength 3.3 GPa) previously wet in a barium osumilite ($BaMg_2Al_6Si_9O_{30}$, BMAS:barium-magnesium-alumina-silicate) precursor glass frit, at ~1,200 °C. During this stage, a weak fibre/matrix interface is formed as a result of chemical reactions occurring between SiC and the oxides of the matrix, providing a carbon-rich layer on the fiber surface [19, 20]. The final volume fraction of fibers in the plates is V_f=0.55. Rectangular beams of dimensions $l \times w \times t = 105 \times 12 \times 3$ mm^3, with and without double-edge notches, were prepared in a CNC vertical machining center using a 300 μm-thick diamond wafering blade (Model 5 LC Diamond Series, Buehler Co. Ltd., Lake Bluff, IL, USA). Fiber orientation in the external plies was set parallel to the loading axis (0°). Notched specimens were prepared with 2 moderately small notch-to-width ratios: 0.2 and 0.35 to allow unfolding of damage mechanisms within the central region. Dogbone specimens were also prepared for pure tension testing according to ASTM C1275-10. Sets of at least 3 specimens were prepared for each test type.

Testing was performed at ambient temperature under crosshead displacement control on an Instron 8800 servohydraulic test system (Illinois Tool Works, Glenview, IL, USA) equipped with a 100 kN load cell and hydraulic clamping grips. Unloading commenced at 10^{-3} strain with a step of 1.5×10^{-3} and specimens were stress-free before commencement of reloading. Loading, unloading and reloading occurred at a constant displacement rate of 0.2 mm/min. A clip-on axial extensometer equipped with knife-edge mounting legs, gauge length 25 mm, was used to record strain on the specimen.

Results and Discussion

The typical mechanical response of double-edge-notched SiC/BMAS composites under cyclic tension, consisted of a linear elastic regime limited within the initial 0.05 % strain which was followed by a regime of gradually decreasing tangent modulus to the curve and decreasing average slope of unloading-reloading cycles indicative of progressive interfacial damage along matrix cracks developing in planes perpendicular to the fibers' axis. Attainment of maximum stress was followed by catastrophic failure of all DEN specimens tested. Composite strength decreased marginally with notch length; average values of 279 and 271 MPa were calculated for specimens of notch-to-width ratios of 0.2 and 0.35, respectively. Composite Young's modulus followed the same trend with average values of 118 and 109 GPa for the above ratios. By examination of the abscissas of unloading curves at zero stress it was observed that notched specimens exhibited limited positive inelastic strain accumulation.

The typical mechanical response of un-notched SiC/BMAS composites, was considerably different in that it exhibited a triple regime behavior and a surprisingly well-defined CIP of unloading-reloading cycles, self-assembled by unloading-reloading data at an average strain of 0.1 % and stress of 90 MPa, as seen in Fig. 1. While the initial elastic and damage regimes were of the same qualitative characteristics as in the notched specimens, the primer appeared to span larger strains for un-notched specimens, namely 0.3 % compared to *ca.* 0.05 % in notched ones. The damage regimes spanned identical strain ranges of 0.3 % in both specimen types. The third regime, with characteristics of macroscopic stiffening such as an almost linear stress–strain relationship and an increase in tangent modulus, appeared after the attainment of a saturated matrix cracking state and corresponded to a material behavior governed by load bearing by intact fibers in a completely bridged matrix environment. Indeed, the purely elastic behavior of fibers in the composite, approximated by a dashed line of slope $\lambda E_f V_f$=52.2 GPa, where λ=0.5 is the non-unidirectional reinforcement correction factor, compares very well to the slope of the final unloading cycle before failure, 52 GPa. Similar stiffening phenomena and linear stress–strain end shapes in composite curves have been reported in the past

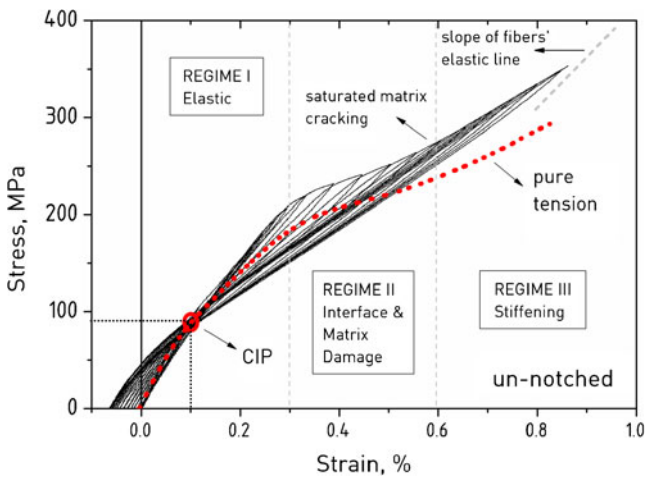

Fig. 1 Typical mechanical response of SiC/BMAS composites under cyclic (*solid line*) and monotonic tension (*dotted line*)

[21–23]. The average strengths and elastic moduli of un-notched composites were 353 MPa and 151 GPa respectively, increased by 28 % and 32 % from the mean corresponding values of notched specimens.

Contrary to DEN specimens, un-notched composites exhibited extended inelastic strain accumulation, of negative sign—arguably due to the expansion of the matrix blocks under residual compression and the corresponding contraction of fibers bridging the cracks that occurs as TRS is relieved during loading [15]. Inelastic strain, plotted in Fig. 2 as a function of peak cycle stress, increased in absolute value within the damage regime and reached a plateau value after the attainment of a saturated matrix cracking state. This finding is in line with the rationale of inelastic strain being closely related to the cracking mechanism.

Independently of specimen type, the shapes of unloading/reloading loops exhibited hysteresis coupled with deviation from linearity of the unloading curve, and introduction of positive curvature. Hysteresis, a result of the sliding conditions and the frictional coefficient at the fiber-matrix interface, is directly related to the residual stress state of the composite constituents. Hysteresis was negligible only with the two initial cycles in all cases, it appeared to increase within the damage regime and remained steady with the stiffening regime. Typical loop forms encountered in each of the three regimes are shown in Fig. 3.

The typical mechanical response of the composite under monotonic tension (Fig. 1, dotted line) exhibited the same qualitative characteristics as the envelopes to the cyclic loading curves. The overall shape and existence of the triple regime was common between the two types of loadings, as also was the strain span of the three regimes. A most interesting finding was that the pure- and cyclic- tension lines intersected exactly at the experimental CIP. At strains higher than the CIP, stress increased less rapidly in the monotonically tested composites, resulting in an observed final increase by 20 % in attainable material stress, attributable to cyclic loading [24].

In the conventional procedure for calculating TRS from the coordinates of the projected CIP, the stress co-ordinate of the CIP is equal to the product of the average axial residual stress in the fibers and their volume fraction, whereas the strain co-ordinate is equal to the axial residual strain in the fibers averaged over the gauge length [15]. By application of the same rationale to the self-assembled CIPs of this study, an average axial residual stress on SiC fibers of 163 MPa is calculated. This experimentally-determined value provides the undisputedly true TRS state of the SiC

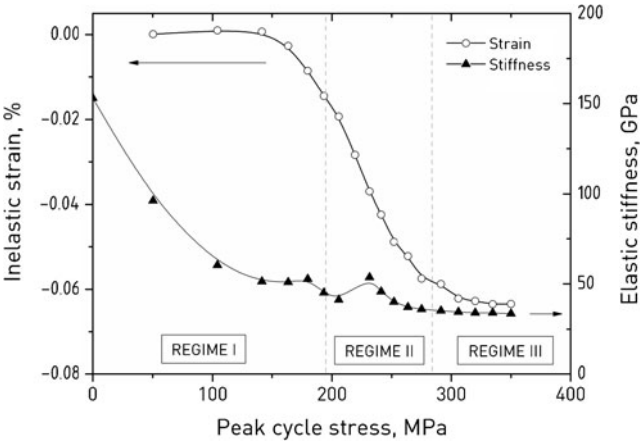

Fig. 2 Evolution of inelastic strain and elastic stiffness of the SiC/BMAS composites during cyclic loading. *Solid lines* represent cubic spline regressions to the data

fibers in the BMAS matrix and can prove helpful in evaluating available TRS-prediction models. Classic theoretical estimations for composites with ideal interfacial bonds, expect the axial residual stress in a non-cracked matrix, σ_r^m, to be:

$$\sigma_r^m = E_m \frac{\lambda E_f V_f}{\lambda E_f V_f + E_m V_m}\left(a_f - a_m\right)\left(T_o - T_p\right) \tag{1}$$

where α_f and α_m are the linear CTEs for the fiber and matrix respectively, while T_o and T_p are the room and processing temperatures, respectively. Using the already known values for E_f, λ and V_f, and E_m=120 GPa [25], $\alpha_f = 4.5\times10^{-6}K^{-1}$ (quoted by manufacturer), $\alpha_m = 2.5\times10^{-6}K^{-1}$ [26], T_o=298 K and T_p=1573 K, the expected axial residual stress in the non-cracked matrix is found to be compressive at 150 MPa. The expected TRS for the fibers would then be tensile at 150 MPa; this value should be considered the theoretical maximum since the source model does not consider the effect of damage mechanisms such as matrix cracking and interfacial debonding that exist in practice. Yet, the true TRS value measured at the assembled CIP, appears 8 % higher than the theoretical prediction. This discrepancy is small considering the accuracy associated with the measurement of the parameters required in equation (1) and shows that this relationship can be used for rough TRS predictions.

Hsueh and Becher have offered a more elaborate analysis for the estimation of axial residual stress on long fibers [27]:

$$\sigma_r^f = A\left\{2\left[\frac{v_f}{E_f} + \frac{V_f v_m}{(1-V_f)E_m}\right]\left(a_m - a_{f,r}\right) + \left[\frac{1-v_f}{E_f} + \frac{1+V_f+(1-V_f)v_m}{(1-V_f)E_m}\right]\left(a_m - a_f\right)\right\}\left(T_o - T_p\right) \tag{2}$$

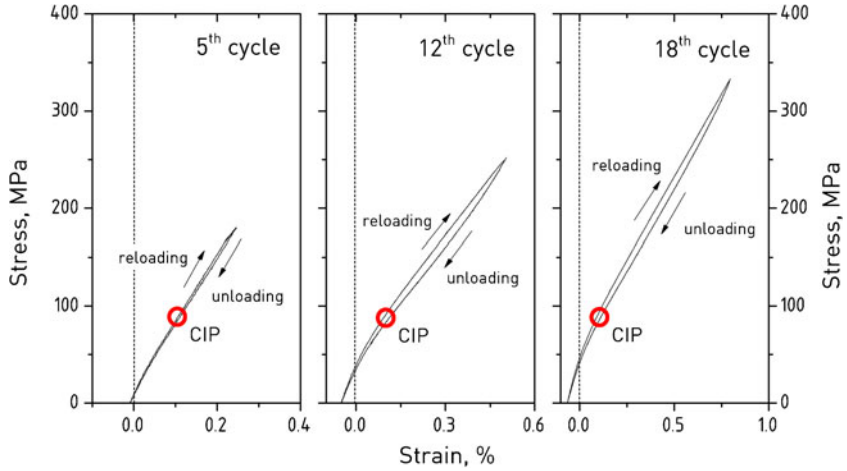

Fig. 3 Evolution of the hysteresis loop shape in the elastic, damage and stiffening regimes

where A is given by:

$$A = \left[\frac{(1+\nu_f)(1-2\nu_f)}{E_f^2} + \frac{V_f(2-\nu_f-\nu_m-4\nu_f\nu_m)+1+\nu_m}{(1-V_f)E_fE_m} + \frac{V_f(1+\nu_m)(1+V_f-2V_f\nu_m)}{(1-V_f)^2E_m^2} \right]^{-1} \quad (3)$$

where $\alpha_{f,r}$ is fiber CTE in the radial direction and ν_f and ν_m are the Poisson's ratios of the fibers and the matrix respectively. Using ν_f=0.15 [28] and ν_m=0.25[25] and two extreme values for the unknown radial CTE of the fibers, $\alpha_{f,r1}$=0 and $\alpha_{f,r}$=4.5×10^{-6}K^{-1}, a range of residual fiber stress of 131 to 205 MPa is calculated. The mean value of this range, 168 MPa compares favorably with the experimentally calculated TRS.

If the CIP is the new TRS-free origin of the mechanical behavior of the composite, it is interesting to investigate the effect of shifting the tensile curve in the stress–strain plane so that the point is brought into coincidence with the origin. By doing so, the composite's Young's modulus in the translated stress/strain domain is recalculated as 104 GPa, a value that is 30 % less than the originally-calculated modulus of 151 GPa and that is now closer to the average modulus of notched specimens, 113 MPa. This finding demonstrates the strong dependence of material properties on residual stresses and indicates the amount of cautiousness that should be taken when calculating properties from mechanical testing data of materials under residual stress. The effect of TRS on properties becomes more complex if machining stresses are considered. The absence of a CIP in the curves of notched specimens signifies that internal residual stresses are relieved in these materials. There are indeed explicit indications that machining damage –in this case removal of material for fabrication of notches normal to the loading direction- is related with the propensity for relaxation of the TRS in both ceramic materials [5, 29] and metal alloys [30].

Knowledge of the experimentally-exact TRS state of the composite can also assist in evaluating the efficiency of the compliance-extrapolation method employed for calculating CIP locations and the associated TRS. While the slope of a particular loop is non-uniquely defined due to the hysteresis effect (Fig. 3) -hence the exact position of the projected CIP depends on the choice of slope and the assumptions therein- the upper part of the reloading modulus (linear end of reloading curve, subset graph in Fig. 4), is widely accepted as the relevant elastic stiffness, equivalent to the modulus of the damaged material under monotonic tension. The regression

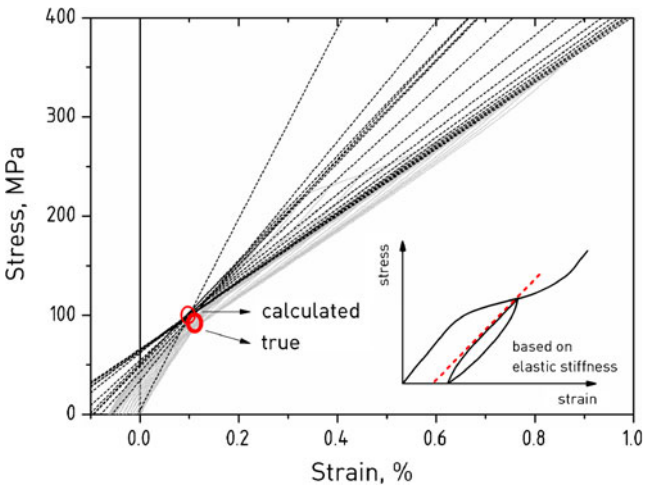

Fig. 4 Evaluation of the CIP-by-compliance calculation method across the true experimental CIP

result to the 17 reloading cycles of Fig. 3 is presented in Fig. 4 as a well-assembled CIP that compares favorably with the location of its experimentally-obtained counterpart. The values of the calculated elastic stiffness, plotted as a function of cycle stress in Fig. 2, appeared to decrease rapidly from the Young's modulus value, 153 GPa, within the initial regime and attain a plateau value of *ca.* 35 GPa near the end of the damage regime. Two transient fluctuations in the otherwise monotonic decrease in the stiffness curve, at cycles near the end of the first regime and soon within the second regime, could be related to the unfolding of energy dissipation phenomena such bridging and interfacial debonding. The stress coordinate of the calculated CIP, 100 MPa, translates to an axial TRS of 181 MPa on the reinforcing fibers, which is 11 % higher than the experimental value and 17 % higher than the TRS predicted by equation (1). A similar analysis, performed on the basis of the unloading slope, indicated a TRS of 90 MPa, which underestimates the true TRS by 44 %. Hence the widely used CIP-by-compliance extrapolation method based on the elastic stiffness (linear reloading slope) proves quite accurate in assessing the actual TRS of the SiC/BMAS composite under investigation.

Conclusions

The average stress coordinates of common intersection points of unloading-reloading loops in the tensile curves of cyclically-loaded SiC/BMAS ceramic matrix composites, were used to directly measure residual tensile stresses of 163 MPa on the reinforcing fibers. The experimentally-exact TRS values were used to test the efficiency of two prominent residual stress models as well as to validate the leading methodology for calculating CIPs through the elastic compliance extrapolation method, for two different moduli choices, either unloading modulus, or reloading modulus. It was found that the compliance method based on the reloading modulus was closer to the true experimental findings as it provided TRS values that were 11 % higher than the directly measured values. The compliance extrapolation method based on the unloading modulus underestimated the experimentally captured behavior by 44 %. The TRS expected under the classical assumption of ideal interfacial bonds, also underestimated the real TRS state by 8 % whereas the results obtained by application of the Hsueh and Becher model compared favorably within 2 % of the experimental value.

References

1. Dassios KG, Aggelis DG, Kordatos EZ, Matikas TE (2013) Cyclic loading of a SiC-fiber reinforced ceramic matrix composite reveals damage mechanisms and thermal residual stress state. Compos A: Appl Sci Manuf 44:105–113
2. Selsing J (1961) Internal stresses in ceramics. J Am Ceram Soc 44:419
3. Young RJ, Yang X (1996) Interfacial failure in ceramic fibre/glass composites. Compos A: Appl Sci Manuf 27:737–741
4. Faber KT (1997) Ceramic composite interfaces: properties and design. Annu Rev Mater Sci 27:499–524
5. Cook RF, Lawn BR, Dabbs TP, Chantikul P (1981) Effect of machining damage on the strength of a glass-ceramic. J Am Ceram Soc 64:C121–C122
6. Kotoul M, Pokluda J, Sandera P, Dlouhy I, Chlup Z, Boccaccini AR (2008) Toughening effects quantification in glass matrix composite reinforced by alumina platelets. Acta Mater 56:2908–2918
7. Serbena FC, Zanotto ED (2012) Internal residual stresses in glass-ceramics: a review. J Non-Cryst Solids 358:975–984
8. Withers PJ, Bhadeshia HKDH (2001) Overview—Residual stress part 1—Measurement techniques. Mater Sci Technol Ser 17:355–365
9. Yang X, Young RJ (1994) Model ceramic fiber-reinforced glass composites—residual thermal-stresses. Composites 25:488–493
10. Dassios KG, Galiotis C (2006) Direct measurement of fiber bridging in notched glass-ceramic-matrix composites. J Mater Res 21:1150–1160
11. Pezzotti G, Sbaizero O, Sergo V, Muraki N, Maruyama K, Nishida T (1998) *In situ* measurements of frictional bridging stresses in alumina using fluorescence spectroscopy. J Am Ceram Soc 81:187–192
12. Guo S, Todd RI (2010) Cr3+ microspectroscopy measurements and modelling of local variations in surface grinding stresses in polycrystalline alumina. J Eur Ceram Soc 30:2533–2545
13. Peitl O, Serbena FC, Mastelaro VR, Zanotto ED (2010) Internal residual stress measurements in a bioactive glass-ceramic using Vickers indentation. J Am Ceram Soc 93:2359–2368
14. Camus G, Guillaumat L, Baste S (1996) Development of damage in a 2D woven C/SiC composite under mechanical loading.1. Mechanical characterization. Compos Sci Technol 56:1363–1372
15. Steen M (1998) Tensile mastercurve of ceramic matrix composites: significance and implications for modelling. Mat Sci Eng A Struct 250:241–248
16. Mei H (2008) Measurement and calculation of thermal residual stress in fiber reinforced ceramic matrix composites. Compos Sci Technol 68:3285–3292
17. Mei H, Cheng LF (2009) Comparison of the mechanical hysteresis of carbon/ceramic-matrix composites with different fiber preforms. Carbon 47:1034–1042
18. Morscher GN, Singh M, Kiser JD, Freedman M, Bhatt R (2007) Modeling stress-dependent matrix cracking and stress–strain behavior in 2D woven SiC fiber reinforced CVISiC composites. Compos Sci Technol 67:1009–1017
19. Cooper RF, Chyung K (1987) Structure and chemistry of fiber matrix interfaces in silicon-carbide fiber-reinforced glass ceramic composites—an Electron-Microscopy Study. J Mater Sci 22:3148–3160
20. Benson PM, Spear KE, Pantano GC (1988) Interfacial characterisation of glass matrix/Nicalon SiC fiber composites: a thermodynamic approach. Ceram Eng Sci Proc 9:663–670
21. Wang M, Laird C (1996) Characterization of microstructure and tensile behavior of a cross-woven C-SiC composite. Acta Mater 44:1371–1387
22. Wang MD, Laird C (1997) Tension-tension fatigue of a cross-woven C/SiC composite. Mat Sci Eng a-Struct 230:171–182
23. Cady C, Evans AG, Perry KE (1995) Stress redistribution around mechanical attachments in ceramic-matrix composites. Composites 26:683–690
24. Mei H, Cheng LF (2011) Stress-dependence and time-dependence of the post-fatigue tensile behavior of carbon fiber reinforced SiC matrix composites. Compos Sci Technol 71:1404–1409

25. Widjaja S (2001) Determination of creep-induced residual stress in fiber-reinforced glass-ceramic matrix composites by X-ray diffraction. Mater Charact 47:47–54
26. Jais US, Lee WE, James PF (1999) Crystallization of barium osumilite glass. J Am Ceram Soc 82:3200–3208
27. Hsueh CH, Becher PF (1988) Thermal-expansion coefficients of unidirectional fiber-reinforced ceramics. J Am Ceram Soc 71:C438–C441
28. Vanwijgenhoven E, Wevers ML, van der Biest O (1999) Influence of the laminate lay-up on the fatigue behaviour of SiC-fibre/BMAS-matrix composites. Compos A: Appl Sci Manuf 30:623–635
29. Johnsonwalls D, Evans AG, Marshall DB, James MR (1986) Residual-stresses in machined ceramic surfaces. J Am Ceram Soc 69:44–47
30. Boyce BL, Chen X, Peters JO, Hutchinson JW, Ritchie RO (2003) Mechanical relaxation of localized residual stresses associated with foreign object damage. Mater Sci Eng A Struct 349:48–58